University of Dundee

# Click-chemistry mediated synthesis of OTBN-1,2,3-Triazole derivatives exhibiting STK33 inhibition with diverse anti-cancer activities

Vala, Disha P.; Dunne Miller, Amy; Atmasidha, Aditi; Parmar, Mehul P.; Patel, Chirag D.; Upadhyay, Dipti B.

Citation for published version (APA):
Vala, D. P., Dunne Miller, A., Atmasidha, A., Parmar, M. P., Patel, C. D., Upadhyay, D. B., Bhalodiya, S. S., González-Bakker, A., Khan, A. N., Nogales, J., Padrón, J. M., Banerjee, S., & Patel, H. M. (2024). Click-chemistry mediated synthesis of OTBN-1,2,3-Triazole derivatives exhibiting STK33 inhibition with diverse anti-cancer activities. *Bioorganic chemistry*, *149*, Article 107485. Advance online publication. https://doi.org/10.1016/j.bioorg.2024.107485

ELSEVIER

# Click-chemistry mediated synthesis of OTBN-1,2,3-Triazole derivatives exhibiting STK33 inhibition with diverse anti-cancer activities

Disha P. Vala [a,1,2], Amy Dunne Miller [b,1,3], Aditi Atmasidha [b,1], Mehul P. Parmar [a,4], Chirag D. Patel [a,5], Dipti B. Upadhyay [a,6], Savan S. Bhalodiya [a,7], Aday González-Bakker [c,8], Adam N. Khan [c], Joaquina Nogales [b,9], José M. Padrón [c,10], Sourav Banerjee [b,*,11], Hitendra M. Patel [a,*,12]

[a] Department of Chemistry, Sardar Patel University, Vallabh Vidyanagar-388 120, Gujarat, India
[b] Department of Cellular and Systems Medicine, School of Medicine, University of Dundee, Dundee DD1 9SY, UK
[c] BioLab, Instituto Universitario de Bio-Orgánica Antonio González, Universidad de La Laguna, Avda. Astrofísico Francisco Sánchez 2, 38206 La Laguna, Spain

## ARTICLE INFO

## ABSTRACT

There is a continuous and pressing need to establish new brain-penetrant bioactive compounds with anti-cancer properties. To this end, a new series of 4′-((4-substituted-4,5-dihydro-1*H*-1,2,3-triazol-1-yl)methyl)-[1,1′-biphenyl]-2-carbonitrile (OTBN-1,2,3-triazole) derivatives were synthesized by click chemistry. The series of bioactive compounds were designed and synthesized from diverse alkynes and $N_3$-OTBN, using copper (II) acetate monohydrate in aqueous dimethylformamide at room temperature. Besides being highly cost-effective and significantly reducing synthesis, the reaction yielded 91–98 % of the target products without the need of any additional steps or chromatographic techniques. Two analogues exhibit promising anti-cancer biological activities. Analogue **4l** shows highly specific cytostatic activity against lung cancer cells, while analogue **4k** exhibits pan-cancer anti-growth activity. A kinase screen suggests compound **4k** has single-digit micromolar activity against kinase STK33. High STK33 RNA expression correlates strongly with poorer patient outcomes in both adult and pediatric glioma. Compound **4k** potently inhibits cell proliferation, invasion, and 3D neurosphere formation in primary patient-derived glioma cell lines. The observed anti-cancer activity is enhanced in combination with specific clinically relevant small molecule inhibitors. Herein we establish a novel biochemical kinase inhibitory function for click-chemistry-derived OTBN-1,2,3-triazole analogues and further report their anti-cancer activity in vitro for the first time.

* Corresponding authors.
*E-mail addresses:* dishuahir1999@gamil.com, disha_pv1999@spuvvn.edu (D.P. Vala), 140001249@dundee.ac.uk (A. Dunne Miller), 2438183@dundee.ac.uk (A. Atmasidha), agonzaba@ull.es (A. González-Bakker), alu0101224077@ull.edu.es (A.N. Khan), jnogalesdiaz002@dundee.ac.uk (J. Nogales), jmpadron@ull.es (J.M. Padrón), s.y.banerjee@dundee.ac.uk (S. Banerjee), hm_patel@spuvvn.edu (H.M. Patel).
[1] Authors contributed equally.
[2] Orcid ID: https://orcid.org/0000-0002-6979-3657.
[3] Orcid ID: https://orcid.org/0009-0003-8712-8444.
[4] Orcid ID: https://orcid.org/0000-0001-6958-8568.
[5] Orcid ID: https://orcid.org/0009-0004-1786-3475.
[6] Orcid ID: https://orcid.org/0000-0001-8027-7330.
[7] Orcid ID:https://orcid.org/0009-0006-2456-7951.
[8] Orcid ID:https://orcid.org/0000-0002-9792-5194.
[9] Orcid ID: https://orcid.org/0000-0002-8195-8362.
[10] Orcid ID: https://orcid.org/0000-0001-6268-6552.
[11] Orcid ID: https://orcid.org/0000-0003-2043-2989.
[12] Orcid ID: https://orcid.org/0000-0003-4740-7329.

# 1. Introduction

Since 2001, over 70 kinase inhibitors have been clinically approved for the treatment of various cancers [1]. While targeting kinases in lung cancer have been especially successful, a large majority of FDA-approved kinase inhibitors have failed in adult glioma and paediatric diffused intrinsic pontine glioma trials [2,3]. Most brain cancer patients exhibit high mortality due to rapid relapse [4,5] and rely on invasive neurosurgery, radiation, and alternative experimental therapies [6] for better end-of-life care. For this purpose, it is essential to consider brain penetrance as an important criterion during future kinase inhibitor drug discovery and medicinal chemistry programmes.

A highly impactful drug synthetic strategy developed over 23 years ago is the click approach [7,8]. Click chemistry has been revolutionary [9,10] in the generation of a wide range of 1,4-disubstitued-1,2,3-triazole compounds with diverse anti-proliferative [11,12], anti-diabetic [13], antimicrobial [14,15] and anti-hypertensive properties [16]. It is a variation of the exergonic Huisgen 1,3-dipolar cycloaddition reaction between terminal acetylenes and azides for the rapid synthesis of five-membered heterocyclic compounds [13,17]. In the initial stages of click chemistry optimization, a copper catalyst was used for the cyclization of two unsaturated starting materials termed copper catalysed azide-alkyne cycloaddition or CuAAC. This powerful strategy has seen extensive applications in drug discovery, material, and polymer science [18]. Indeed, a ground-breaking study [19] reported a strained promoted [3 + 2] cycloaddition reaction based on CuAAC which allowed for selective modification in biomolecules with excellent biorthogonality and without physiological harm. 1,2,3-triazoles are very useful either as building blocks for the synthesis of drug intermediates [20] or in applications such as bio-isostere of amide, carboxylic acid and ester [21,22]. In the current study, we utilised this revolutionary click approach to synthesise a new class of 1,2,3-triazole-OTBN analogous which exhibited diverse anti-cancer properties. We coupled substituted 4-bromo-OTBN and 1,2,3-triazole moiety to successfully generate anti-cancer derivatives with predicted brain penetrance. In fact, the most potent pan-cancer analogue exhibited specific serine threonine kinase STK33 inhibitory function within a panel of 139 kinases. STK33 has been targeted, albeit controversially, as a synthetic lethal oncogene in KRAS dependent cancer [23,24]. For this purpose, a few inhibitors for STK33 have been reported previously but none have entered the clinic yet. We further show that STK33 is indeed a true drug target and is highly expressed in glioblastoma which in turn correlates with poorer survival in patients.

Herein, we report the design and synthesis of a potent and potentially brain-penetrant 1,2,3-Triazole-OTBN drug intermediate using a simple, green, and efficient click-chemistry protocol exhibiting potent anti-brain cancer activity with STK33 kinase-inhibitory properties.
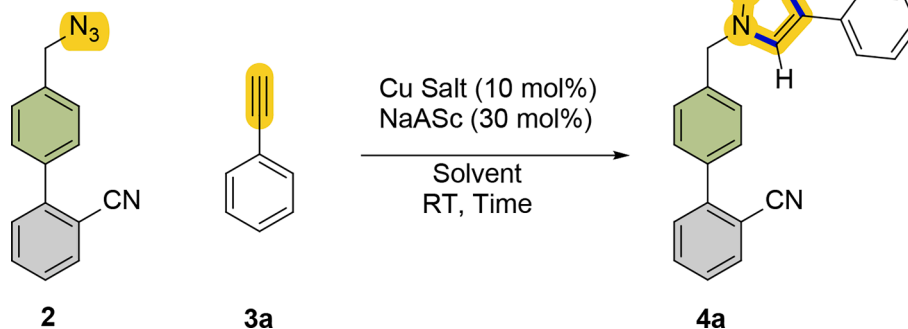
# 2. Result and discussion

## 2.1. Chemistry
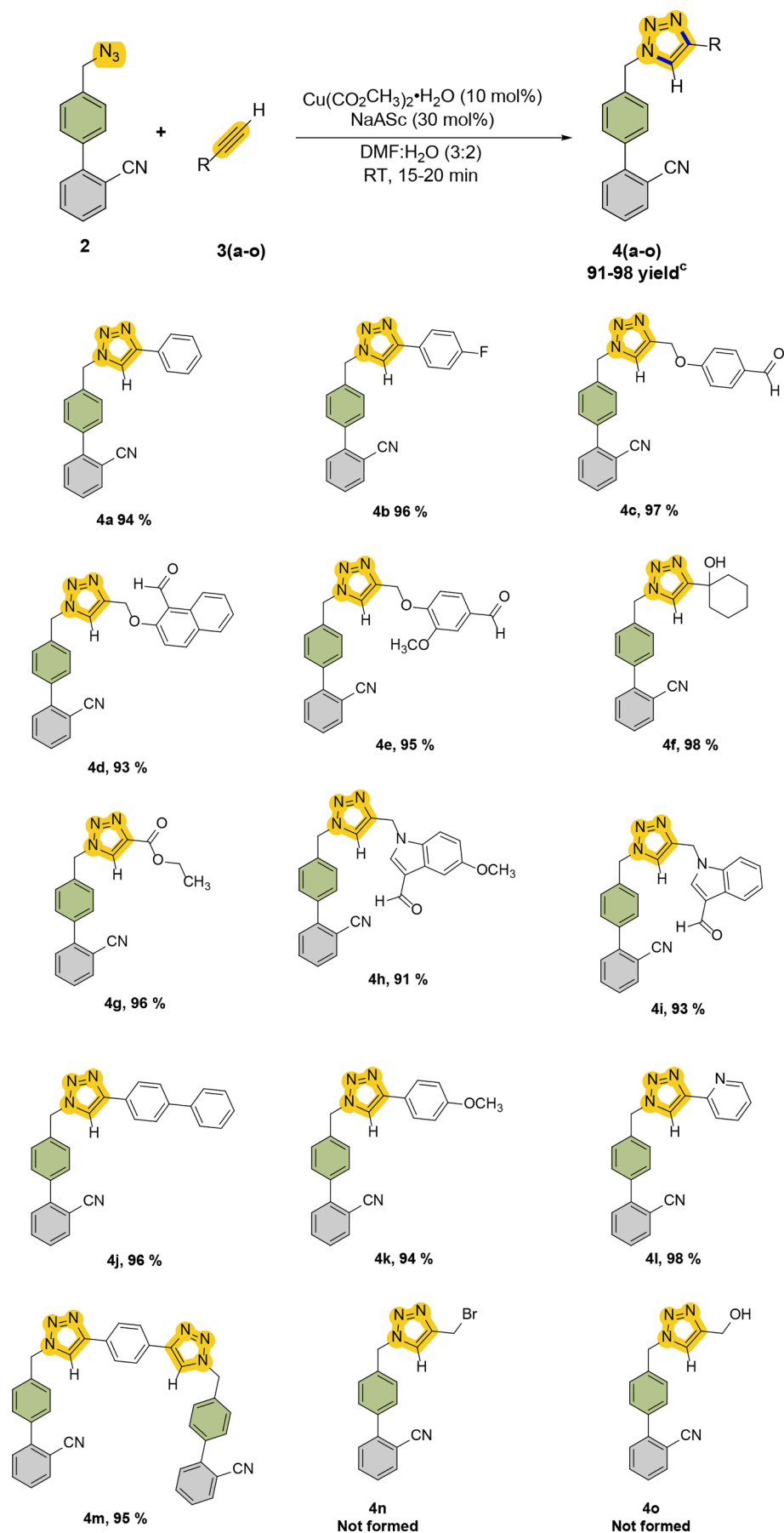
Optimization of reaction[a]

To optimise reaction parameters, we conducted a series of reactions between azide **2** and phenylacetylene **3a** as a model, using Cu(I) iodide (10 mol%) as a catalyst, NaASc as an additive and DMF as a solvent, at room temperature. We were glad to see the formation of triazole as the only reaction product with a 100 % conversion yield with respect to azide **2** within 25 min (entry 1) on our first attempt. While acetone, methanol, acetonitrile, and water failed as solvents (entries 2–5), DMSO completed the reaction within 25 min as well (entry 6). After optimising the solvent, the reaction was performed using various catalysts such as $CuSO_4 \cdot 5H_2O$, $CuCl_2$, $Cu(OTf)_2$, and Copper (II) acetate monohydrate. The Displacement of CuI with $CuCl_2$ and $Cu(OTf)_2$ (entries 8,9) led to failures and lower yield respectively. On the other hand, $CuSO_4 \cdot 5H_2O$ with NaASc took 40 min (entry 7) and surprisingly copper (II) acetate monohydrate took only 15 min with a 100 % conversion yield with respect to azide **2** (entries 10) (Scheme 1).

Our 4′-(azidomethyl)-[1,1′-biphenyl]-2-carbonitrile **2** was synthesized from 4′-(bromomethyl)-[1,1′-biphenyl]-2-carbonitrile (Bromo-OTBN) **1** and sodium azide ($NaN_3$) in DMF for 14–18 hrs at room temperature (25–30 °C) (Scheme 2).

The reactions with 4′-(azidomethyl)-[1,1′-biphenyl]-2-carbonitrile **2** and different terminal alkynes such as **3(a-o)** using commercially readily available copper (II) acetate monohydrate catalyst and NaASc (30 mol %) reached a 100 % conversion yield with respect to azide **2** within 15 min using DMF: $H_2O$ (3:2) 5 ml (Scheme 3). The desired crude products **4(a-m)** precipitate out with water. These crude products **4(a-m)** were filtered and washed first with (2 × 25 ml) water and then (2 × 10 ml) ethyl acetate: *n*-hexane (10:90). Copper (II) compound is used as a
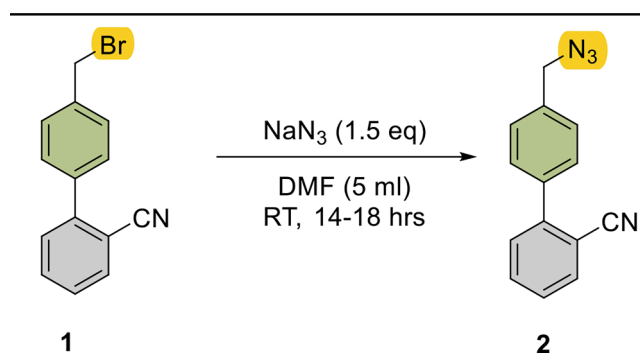


**Scheme 2.** Synthesis of compound **2**. [a]Reaction condition: 1mmol 4'-(bromo-methyl)-[1,1'-biphenyl]-2-carbonitrile **1** and 1.5 mmol Sodium azide, 5 ml DMF, RT, 14-18 hrs.



**Scheme 1.** Optimization reaction conditions.

**Scheme 3.** Substrate scope of Reaction.

**Table 1**
Optimization conditions.

| Entry | Cu Salt | Solvent | Time (t) | %Conv [b] |
|-------|---------|---------|----------|-----------|
| 1 | CuI | DMF | 25 min | 100 |
| 2 | CuI | Acetone | 24 hrs | No reaction |
| 3 | CuI | Methanol | 24 hrs | No reaction |
| 4 | CuI | Acetonitrile | 24 hrs | No reaction |
| 5 | CuI | Water | 24 hrs | No reaction |
| 6 | CuI | DMSO | 25 min | 100 |
| 7 | CuSO$_4$·5H$_2$O | DMF:H$_2$O (3:2) | 40 min | 100 |
| 8 | CuCl$_2$ | DMF:H$_2$O (3:2) | 18 hr | 75 |
| 9 | Cu(OTf)$_2$ | DMF:H$_2$O (3:2) | 18 hr | 95 |
| 10 | **Cu(II) acetate monohydrate** | **DMF:H$_2$O (3:2)** | **15min** | **100** |

[a]Reaction condition: 1 mmol 4′-(azidomethyl)-[1,1′-biphenyl]-2-carbonitrile **2**, 1 mmol phenyl acetylene **3a**, 10 mol% Catalyst, 30 mol% NaASc and 5 ml solvent.

[b] Observed from TLC analysis.

catalyst with an excellent metal reductant, NaASc, which reduces Cu(II) to Cu(I) efficiently.[25] The advantage of generating these *in situ* Cu(I) species eliminates the need for the base. Otherwise, Cu(I) species requires Acetonitrile as a co-solvent and a Nitrogen base for the reaction. [7] Therefore, we placed the reducing agent NaASc with Cu(I) catalyst in case Cu(I) oxidizes to Cu(II). This reaction only took and 25 min to complete (Table 1 entry 1).

Under the optimized reaction conditions, the scope concerning terminal alkynes was examined. Almost all alkynes gave excellent yield with azide **2** but, propargyl bromide **3n** and propargyl alcohol **3o** did not give a reaction. Under the standard one-pot reaction conditions, the reaction takes a longer time (24–48 hrs) with high catalyst loading (20–30 mol%). Herein, alkynes **3(c-e) and 3(h-i) were** synthesised using a previously reported method [26], parting from –OH and –NH containing compounds (1 mmol) respectively, using Propargyl bromide (1.2 mmol) K$_2$CO$_3$ (3 mmol) as a base and DMF (4 ml) as a solvent.

### 2.2. Crystal data and structure refinement for Compound 2

To develop a single crystal, 150 mg of compound **2** was dissolved in 100 ml ethyl acetate and heated until compound **2** was properly dissolved and the amount of solution was halved (50 ml). Following this, 150 mg of activated charcoal was added to eliminate coloured impurities from the compound. Once the charcoal treatment solution was filtered, it was kept in a clean beaker covered with aluminium foil for a couple of days. When the ethyl acetate was evaporated, a single crystal of compound **2** developed over 10–15 days. It developed into a colourless rectangular form with the approximate dimensions of 0.250 mm × 0.220 mm × 0.180 mm.

Compound **2** crystallised (Fig. 1**A & 1B**) with the triclinic crystal system, space group p-1, and unit cell parameter: a = 8.0204(7) Å, b = 8.1641(8) Å, c = 10.0523(9) Å, α = 76.322(4)°, β = 69.458(4)°, γ = 86.20(4)°and Z = 2. The density was calculated at 1.299 g/cm$^3$. The single crystal image, ORTEP diagram, unit cell, and packing configurations are shown below, and other observed data for the single crystal investigation are shown in Table 2.

### 2.3. Biological activity

#### 2.3.1. Identifying key cancer-specific and pan-cancer lead OTBN derivatives

The antiproliferative activity of compounds **2** and **4(a-m)** was studied in a panel of human solid tumour cell lines. The results indicate 50 % growth inhibition − obtained using the well-known protocol of the NCI [27] − and are listed in Table 3. All compounds were able to induce antiproliferative effects on at least one cell line of the panel. The precursor compound **2** was active against most cell lines and showed GI$_{50}$ values in the range 18–32 μM except GBM143. Thus, the potency of

**Table 2**
Crystal data and structure refinement for compound 2.

| Crystal description | Colourless |
|---------------------|------------|
| Crystal Size | 0.250 × 0.220 × 0.180 mm |
| Empirical formula | C$_{14}$H$_{10}$N$_4$ |
| Formula weight | 234.26 |
| Radiation, Wavelength | Mo *K*α, 0.71073 Å |
| Unit cell dimension | a = 8.0204(7) Å α = 76.322(4)° |
| | b = 8.1641(8) Å β = 69.458(4)° |
| | c = 10.0523(9) Å γ = 86.20(4)° |
| Crystal system | Triclinic |
| Space group | p-1 |
| Unit cell volume | 598.82(10) Å$^3$ |
| No. of molecule per unit cell, Z | 2 |
| Temperature | 296(2) K |
| Absorption coefficient | 0.082 mm$^{-1}$ |
| F(000) | 244 |
| Scan mode | Multi-scan |
| θ range for the entire data collection | 2.22 to 26.82° |
| Density (calculated) | 1.299 |
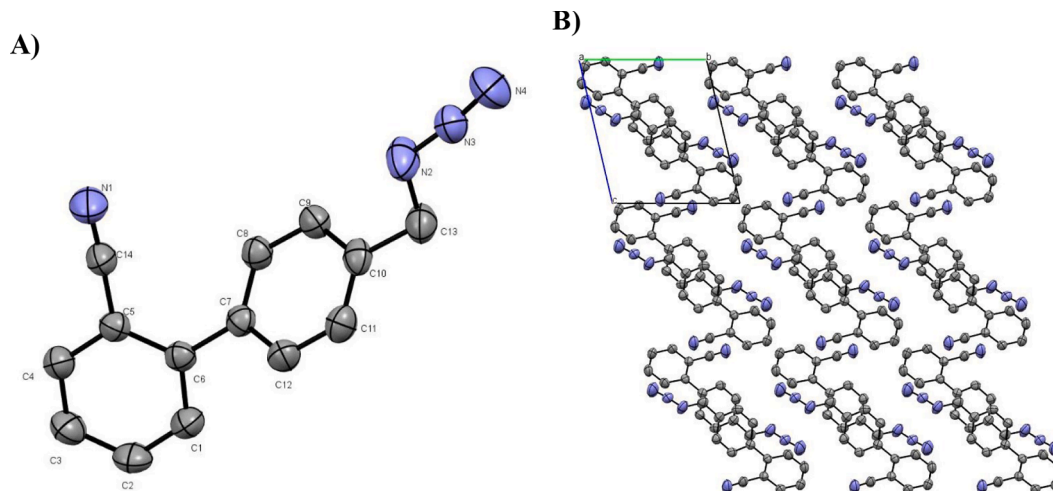


**Fig. 1.** A) The molecular structure of compound **2**. Showing the atom-labelling scheme and displacement ellipsoids at a 50% probability level. B) The packing diagram for compound **2** view along the a-axis.

**Table 3**
Antiproliferative activity (GI$_{50}$, μM) against human tumour cell lines and non-cancerous RPE1 cells.

| Compound | Cell line (origin) | | | | | | | |
|---|---|---|---|---|---|---|---|---|
| | A549 (lung) | HBL100 (breast) | HeLa (cervix) | SW1573 (lung) | T-47D (breast) | WiDr (colon) | GBM143 (brain) | RPE1 (normal) |
| **2** | 32 ± 11 | 27 ± 5.0 | 18 ± 5.1 | 21 ± 5.7 | 29 ± 4.3 | 27 ± 11 | >50 | >50 |
| **4a** | 3.9 ± 1.5 | >50 | >50 | 3.7 ± 1.0 | >50 | >50 | >50 | >50 |
| **4b** | 5.6 ± 1.3 | 9.8 ± 1.5 | 28 ± 13 | 3.5 ± 1.0 | >50 | 35 ± 9.0 | >50 | >50 |
| **4c** | 25 ± 5.3 | 34 ± 5.3 | 25 ± 5.5 | >50 | >50 | >50 | >50 | >50 |
| **4d** | 9.5 ± 4.3 | 24 ± 8.8 | 7.2 ± 2.6 | >50 | >50 | >50 | >50 | >50 |
| **4e** | >50 | 33 ± 11 | 25 ± 6.0 | 45 ± 17 | >50 | >50 | >50 | >50 |
| **4f** | 20 ± 4.9 | 40 ± 16 | 43 ± 20 | 6.5 ± 1.5 | >50 | 33 ± 9.0 | >50 | >50 |
| **4g** | 6.8 ± 3.0 | 13 ± 2.5 | 21 ± 0.8 | 1.4 ± 0.6 | 28 ± 3.5 | 20 ± 7.8 | >50 | >50 |
| **4h** | 3.8 ± 1.0 | 7.7 ± 2.7 | 3.2 ± 0.8 | 5.8 ± 0.6 | 40 ± 19 | 20 ± 7.1 | >50 | >50 |
| **4i** | >50 | >50 | >50 | >50 | >50 | >50 | >50 | >50 |
| **4j** | 19 ± 0.2 | 25 ± 1.0 | 25 ± 0.2 | >50 | >50 | 40 ± 17 | 22.4 ± 2.7 | >50 |
| **4k** | **3.6 ± 0.9** | **4.1 ± 1.7** | **2.6 ± 0.8** | **5.2 ± 0.6** | **3.5 ± 0.6** | **4.1 ± 0.7** | **4.9 ± 0.7** | >50 |
| **4l** | **5.3 ± 1.3** | >50 | >50 | **4.4 ± 0.6** | >50 | >50 | >50 | >50 |
| **4m** | >50 | >50 | 6.0 ± 2.5 | >50 | >50 | >50 | >50 | >50 |
| **cisplatin** | 4.9 ± 0.2 | 1.9 ± 0.2 | 1.5 ± 0.5 | 2.7 ± 0.4 | 17 ± 3.3 | 23 ± 4.3 | 11.4 ± 1.4 | >50 |

[a]Values represent mean ± standard deviation of two to three independent experiments.
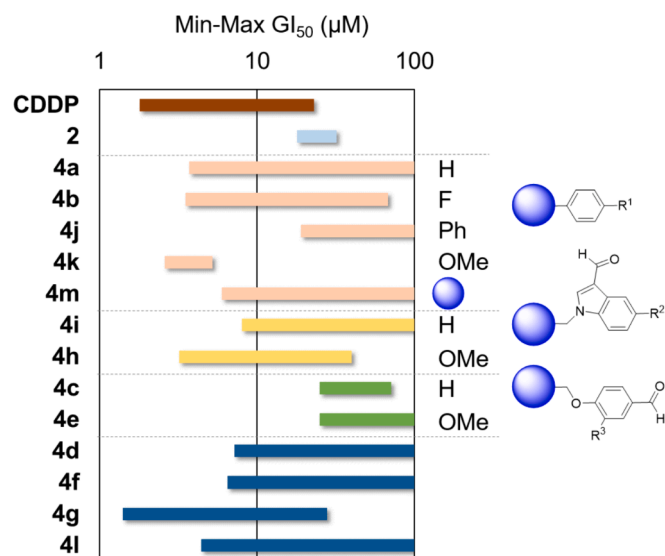


**Fig. 2.** GI$_{50}$ range plot. Partial SARs can be inferred after subclassifying the compounds according to the motif at C4 of the triazole. CDDP: cisplatin.

compound **2** is considered modest. The reaction of compound **2** with alkynes provided triazole derivatives **4(a-m)** which displayed diverse antiproliferative activities when compared to the parent compound. It was not possible to establish global structure activity relationships (SARs) from the results. With the aid of the GI$_{50}$ range plot (Fig. 2), some partial SARs are encountered when considering the motif at C4 of the triazole group. The C4-phenyl derivative **4m** is the "dimeric" version of compound **4a**, which was active against the lung cancer cell lines (GI$_{50}$ = 3.9 μM for A549 and 3.7 μM for SW1573) and weakly against HeLa (~90 μM). This result suggests that the addition of a second biphenyl triazole group (**4m**) produces notable changes in selectivity. Interestingly, **4m** was active exclusively against HeLa cells (GI$_{50}$ = 6.0 μM), suggesting differential selectivity toward cancer cell lines. Compound **4l** displayed antiproliferative effects primarily against the lung cancer cell lines A549 and SW1573, with GI$_{50}$ values of 5.3 and 4.4 μM, respectively with no activity against any of the other cells tested up to 100 μM. Overall, the most active compound of the series was **4k**, with GI$_{50}$ values in the range 2.6–5.2 μM and active against all cell lines tested. It is important to note that none of the drugs had any measurable toxicity against non-cancerous immortalised epithelial hTERT-RPE1 cells, suggesting a viable therapeutic window for the molecules. We utilised cisplatin (CDDP) as a control chemotherapeutic drug as a benchmark for the GI$_{50}$ values of the compound series (Table 3 & Fig. 2).

Since **4l** was remarkably lung cancer-specific while **4k** was a highly potent pan-cancer molecule, we decided to test both derivatives in
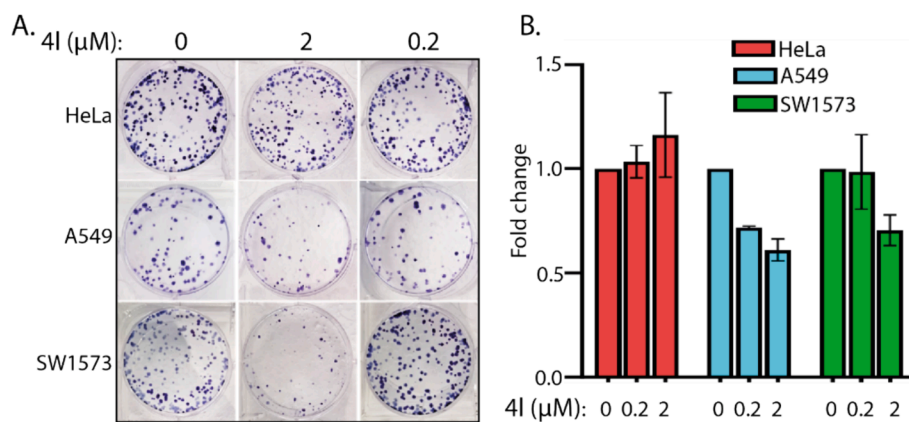


**Fig. 3.** **4l** exhibits lung cancer specific cytostatic activity. (A) Colony formation assay of HeLa, A549 and SW1573 cells exposed to **4l**. Representative crystal violet staining of the colonies formed after seven days of incubation. (B) Relative quantification of optical density of crystal violet content of the indicated treatments. Also see Supplementary Videos 1&2.
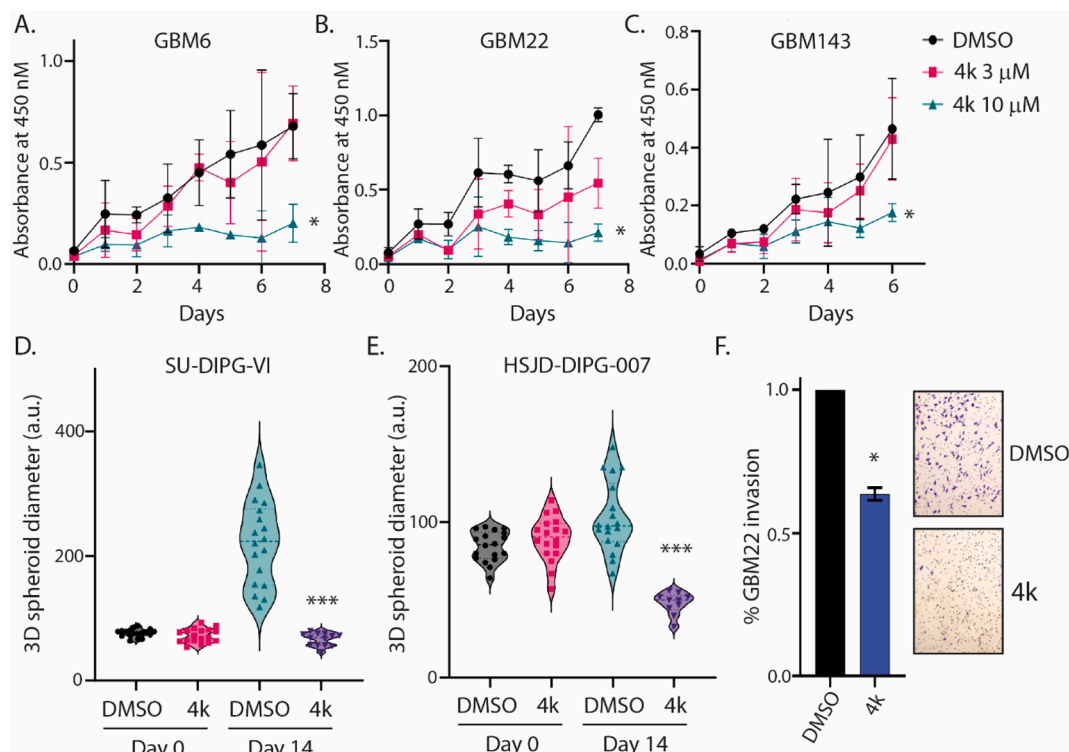
**Fig. 4. 4k** inhibits primary glioma growth in vitro. Growth curves of (A) GBM6, (B) GBM22, (C) GBM143 DMSO control- and **4k**-treated cells. *$P < 0.05$ (2-way ANOVA, mean $\pm$ SD, Tukey's multiple comparisons from $n = 3$ replicates). (D) Paediatric SU-DIPG-VI glioma stem cells were treated with either DMSO or 10 μM **4k** for 14 days and neurospheres were allowed to form. The diameter of the neurospheres were quantified using ImageJ. The significance of the differences was measured using one-way ANOVA with Tukey's multiple comparisons. ***$< 0.001$. (E) Pre-formed paediatric HSJD-DIPG-007 glioma stem neurospheres were treated with either DMSO or 10 μM **4k** for 14 days and the diameter of the neurospheres were quantified as in (D). (F) Bar graph depicting cell invasion in a Matrigel transwell migration assay using DMSO treated or 10 μM **4k** GBM22 cells. Data were acquired 18 h after seeding in upper chamber of 8 μm pore size transwells. Cells that invaded the Matrigel were stained by crystal violet and counted. Data was represented as percent of DMSO-treated. *$P < 0.05$ (compared to DMSO treated, student's *t*-test, mean $\pm$ SD from $n = 2$ independent experiments with duplicates in each). Representative crystal violet stained invasion assay image provided.

further cell-based and biochemical assays. Owing to the strong anti-proliferative activities of **4k** and **4l** OTBN-triazole analogues, their drug-likeness was assessed through ADME (Absorption, Distribution, Metabolism, and Excretion) prediction. **4k** and **4l** have drug-like properties with a bioavailability score of 0.55 (**Table S2**, Supporting information). Furthermore, according to the PAINs and Brenk model, there was no predicted toxicity reported for **4k** and **4l**. Both the derivatives fall within the threshold value of the physicochemical properties by following Lipinski's rule of five, Ghose's, Veber's, Egan's and Muegee's rules (**Table S2**, Supporting information). No violation of any of these rules provides confidence that **4k** and **4l** could indeed be important drug candidates. Also, the cut-off values of certain parameters like molecular weight (MW), topological polar surface area (TPSA), molar refractivity (MR), rotational bond (RB), number of H-bond acceptor [28] and number of H-bond donor (HBD) lie in the acceptable range for OTBN-triazole derivative **4k** and **4l**. In order to predict the blood–brain barrier permeability and high gastrointestinal absorption for the synthesized OTBN-1,2,3-triazole derivatives, **4k** and **4l** 'boiled-egg' depiction was used (**Figure S30**), supporting information)[29]. Both **4k** and **4l** show potential for blood–brain barrier permeability with predictive low gastrointestinal absorption. The blue dots in the yellow (yolk) region report that **4k** and **4l** are PGP + substrates which is one area of improvement that we plan to pursue in the future.

*2.3.2. Lung-cancer specific 4l is cytostatic in function*

Based on the selectivity of compound **4l** toward the lung cancer cell lines, we selected this compound for further testing. To get insight on the mode of action we considered studying the long-term effects of **4l**. The clonogenic assay, the "gold standard" method to measure the sum of all

modes of cell death, encompasses both early and late events such as delayed growth arrest. Therefore, the colony formation assay was carried out (Fig. 3). As a rule of thumb, cells were exposed to two drug doses, 2 and 0.2 μM, based on the GI$_{50}$ values reported in Table 3. After seven days of treatment, the ability to form colonies decreased significantly in A549 and SW1573 cells. In contrast, HeLa cells, not sensitive to **4l** (Table 3), were not affected in their growth. To follow the mode of action of **4l**, SW1573 cells were exposed to **4l** at 20 μM and monitored every five minutes for a total time of 20 h (Videos S(1–2)). The live cell imaging provides insight on cytostatic [30] or cell death effects [31–34] for each individual cell within a population. The analysis after segmentation of the single cells indicated that compound **4l** prevents cell growth without inducing toxic effects to the cells. This suggested that **4l** is a cytostatic compound at the indicated concentrations.

*2.3.3. Establishing the function of 4k compound in brain cancer*

4 K compound presents anti-cancer properties against several types of cancer including brain cancer or GBM. Because **4k** has shown to be a blood–brain barrier permeabile molecule, we further characterized **4k** in different brain cancer cells

*2.3.3.1. Establishing anti-proliferative activity of 4k in GBM.* To further determine **4k**'s anti-proliferative capacity, primary glioblastoma cell lines were treated with DMSO or **4k** (3 μM or 10 μM). A significant decrease in proliferation was observed in all three primary glioma cells following treatment with 10 μM **4k** compared to DMSO control (Fig. 4A-C). While 3 μM **4k** was sufficient to cause a modest decrease in proliferation of GBM6 (Fig. 4A) and GBM143 (Fig. 4C). GBM22 showed highest sensitivity with moderate decrease in proliferation at the lower
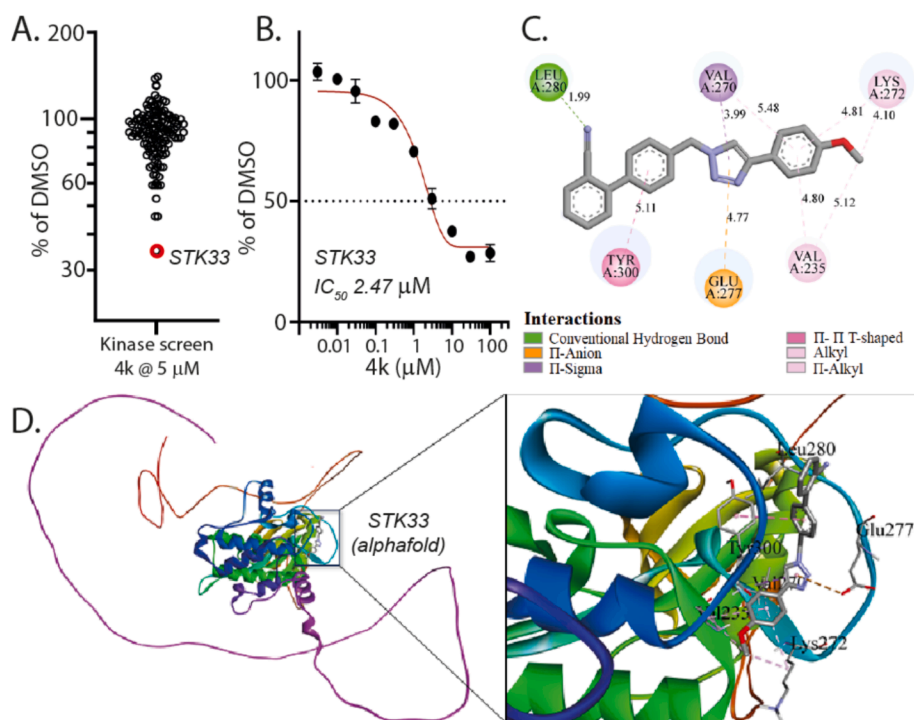
**Fig. 5. 4k** exhibits biochemical inhibitory activity against STK33 (A) Kinase profiling of **4k** at 5 μM was carried out against the panel of 139 kinases at the International Centre for Protein Kinase Profiling (http://www.kinase-screen.mrc.ac.uk/). The IC$_{50}$ value of **4k** was recorded in vitro using purified STK33 (B) over different **4k** concentrations. **4k** was docked into the alphafold-predicted structure of STK33 to identify potential interacting residues in the kinase domain. (C) Interaction diagram of **4k** with STK33. (D) **4k** was docked into the alphafold-predicted structure of STK33 to identify potential interacting residues in the kinase domain.

**4k** concentration. This anti-proliferative capacity was investigated further using two distinct 3D patient-derived paediatric glioma models. A diffuse intrinsic pontine glioma cell line (SU-DIPG-VI) was treated with 10 μM **4k** or DMSO and allowed to form 3D neurospheres. **4k** treatment greatly reduced 3D neurosphere formation in a 2-week period (Fig. 4**D**). Additionally, a large reduction in size was observed in pre-formed 3D HSJD-DIPG-007 neurospheres following a 2-week treatment with **4k** (Fig. 4**E**). Furthermore, 3 μM **4k** can significantly decrease invasion of GBM22 in 24 h (Fig. 4**F**) [35]. Therefore, **4k** shows promise as a treatment for brain-tumours with both anti-proliferative and anti-invasive capacities.

*2.3.3.2. Pan-cancer compound 4k specifically inhibits STK33 in vitro.* To identify any potential kinase inhibitory activity of **4k**, 5 μM **4k** was screened over 139 purified kinases at the International Centre for Protein Kinase Profiling, University of Dundee, UK [36–39]. Interestingly, **4k** significantly inhibited STK33 with a high degree of specificity (Fig. 5**A**). Biochemical IC$_{50}$ analyses were conducted on purified STK33 for **4k**. **4k** exhibited IC$_{50}$ of 2.47 μM for STK33 (Fig. 5**B**). To further predict **4k** binding to STK33, in silico binding studies were conducted (Fig. 5**D**). STK33 crystal structure was not available so the predicted Alphafold structure was used for the in silico docking studies [40]. The results of this analysis show that **4k** has a binding affinity of −8.8 kcal mol$^{-1}$ to STK33. **4k** shows six different types of interactions with the protein such as conventional hydrogen bond, Π-Π *T*-shaped, Π-Anion, Alkyl, Π-Sigma, and Π-Alkyl types of interactions (Fig. 5**C**). One of the *N*-atom of the triazole ring shows hydrogen bonding with Leu280 at 1.99 Å while one of the phenyl rings of the OTBN group interacts relatively weakly with Tyr300 at 5.11 Å through a Π-Π *T*-shaped type of bond. The triazole ring of **4k** itself shows Π-Anion and Π-Sigma type of interactions with Glu277 (4.77 Å) and Val270 (3.99 Å), respectively. The phenyl ring of the p-methoxyphenyl group attached to one of the C-atom of the triazole ring shows Π-Alkyl types of weak interactions with Val235

(4.80 Å), Val270 (5.48 Å), and Lys272 (4.81 Å), respectively. The –CH$_3$ of the p-methoxyphenyl group shows alkyl interactions with Lys272 (4.10 Å) and weakly with Val235 (5.12 Å), respectively. These interactions make the binding of **4k** strong enough in the active site of STK33.

*2.3.3.3. STK33 expression correlates with poorer prognosis in brain cancer.* To understand the expression of STK33 across various cell states of diverse cancers, we queried previously published single-cell RNA sequencing datasets of cancer (https://singlecell.broadinstitute.org/single_cell) [41,42]. Data are represented with either *t*-distributed stochastic neighbour embedding (*t*-SNE) clustering or uniform manifold approximation and projection (uMAP). STK33 RNA expression was highest in the tumour cell population in adult and paediatric glioblastoma with minimal expressions in colon, renal, and breast cancer datasets (Fig. 6**A**). Indeed, higher STK33 expression correlated with poorer outcome for low grade glioma patients (Fig. 6**B**) while glioma and low-grade tumours had higher expression of STK33 than the normal tissue controls (Fig. 6**C**). It is important to note that brain cancers are highly refractory and heterogenous tumours and any novel therapeutic option would be highly impactful [4,5].

*2.3.3.4. Combination with clinically relevant brain-penetrant drugs.* To further establish the ability of **4k** to induce cytotoxicity in cancer cells, we tested it in combination with clinically relevant brain-penetrant small molecules. We tested **4k** in combination with PI-103, buparlisib, abemaciclib, bozitinib, marizomib, nilotinib, and osimertinib as reported previously [43]. In combination with PI3K and MET inhibitory molecules, as well as a proteasome inhibitor, **4k** exhibited potent growth inhibition of GBM6 cells (Fig. 7**A-D**). However, no additive or synergistic growth inhibition was observed for **4k** in combination with abemaciclib, nilotinib, and osimertinib (Fig. 7**D-G**). These results suggests that brain-penetrant derivatives of **4k** could be used in combination with
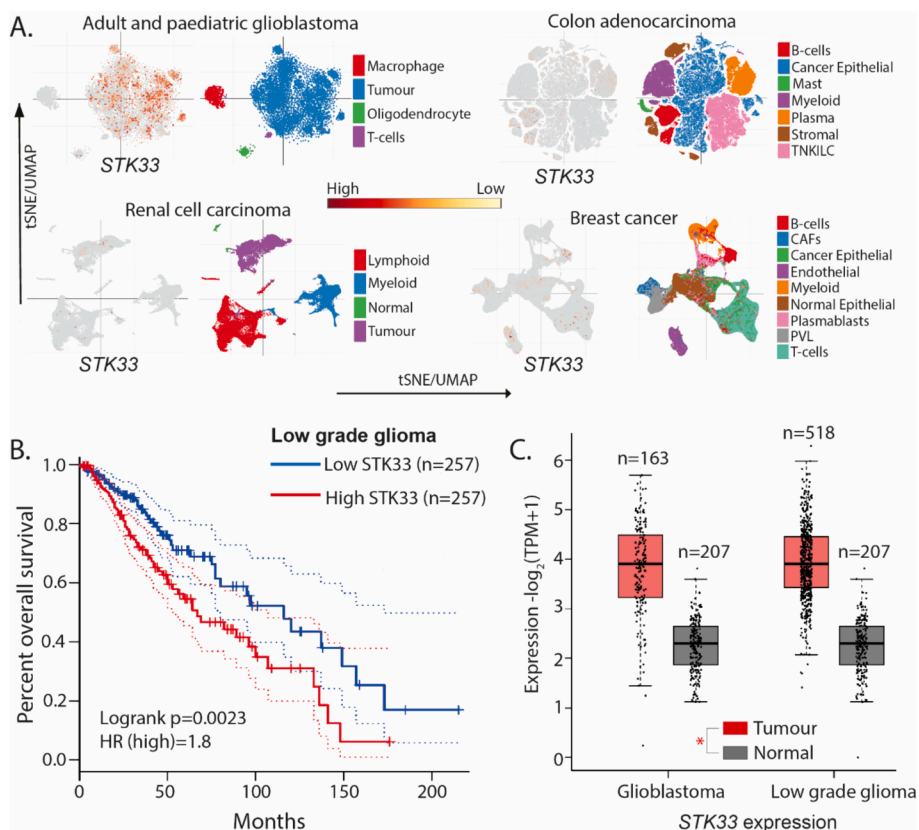
**Fig. 6.** STK33 is highly expressed in glioma. (A) RNA expression of STK33 overlayed on the tSNE or UMAP distribution of previously published sc-RNAseq datasets for adult and paediatric glioblastoma, colon adenocarcinoma, renal cell carcinoma, and breast cancer. (B) STK33 higher expression corelates with poor overall survival in low grade glioma patients. (C) High grade and low-grade glioma tumour samples exhibit higher expression of STK33 compared to normal brain controls (*p < 0.05).
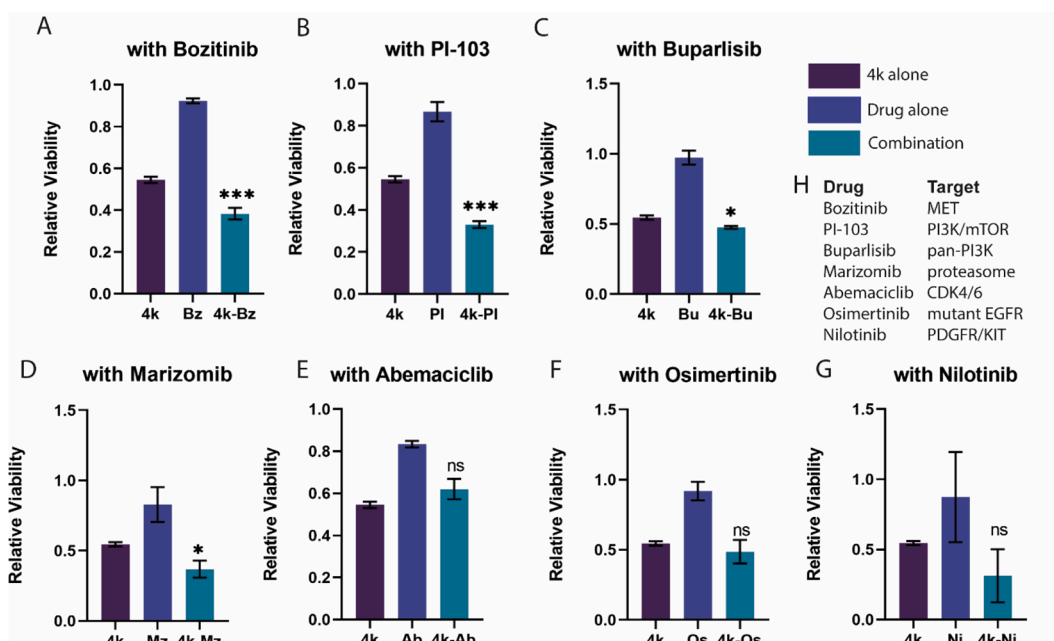


**Fig. 7.** **4k** induces enhanced cell growth inhibition in combination with specific clinically relevant brain-penetrant small molecule inhibitors. GBM6 cells were treated with **4k** alone (10 μM) or clinical drugs alone (A) Bozitinib 7 μM, (B) PI-103 100 nm, (C) Buparlisib 500 nm, (D) Marizomib 400 nM, (E) Abemaciclib 1 μM, (F) Osimertinib 2 μM, (G) Nilotinib 5 μM, or a combination of both for 72 h. Cell viability was analysed and data represented as fold viability of DMSO-treated control for each cell line. A one-way ANOVA with Fisher's LSD test was carried out for each combination (* p < 0.05, *** p < 0.001, ns: not significant, n = 3). (H) Table lists the cellular targets of the respective clinically relevant brain-penetrant drugs.

receptor-tyrosine kinase or proteasome inhibitors to treat brain tumours.

## 3. Conclusion

Herein, we synthesise a new series of OTBN-1,2,3-triazole analogues using green routes, economically favorable and readily available Copper (II) acetate monohydrate within 15 min reaction time. These analogues can be used as intermediates to create molecular libraries of bioactive functionalised 1,2,3-triazole compounds. Initial screening identified two promising candidates: **4k** as a pan-cancer drug and **4l** as lung cancer specific drug. Neither **4k** nor **4l** exhibited any cytotoxicity against non-cancerous RPE cells. **4l** was confirmed as lung-cancer specific cytostatic drug with excellent potential for future use as lung-cancer treatment in combination with existing cytotoxic therapies. On the other hand, it was found that **4k** inhibits STK33 with high specificity. High STK33 expression has been shown to correlate with progression of several cancer types [44–47]. Indeed, bioinformatic analysis from the single-cell RNA sequencing database showed that STK33 was highly expressed in paediatric and adult glioblastoma, correlating with poor patient prognosis. This suggests that the need for STK33 inhibitors is particularly pronounced in the case of glioblastoma. Analogue **4k** reduced proliferation in all three-glioblastoma cell-lines significantly with the extent of this effect being cell-specific. Furthermore, **4k** targets stemness as treatment reduced both the size of formed and forming neurospheres, a 3D stem-like model. **4k** also led to a decrease in invasion indicating STK33 inhibition could reduce tumour spreading. However, due to the heterogeneous nature of glioblastoma, inhibition of one kinase may not be sufficient. Combination of **4k** with Bozitinib, PI-103 and Buparlisib showed the largest anti-cancer effects, two of these are PI3K inhibitors – suggesting that dual STK33 and PI3K inhibition is a potent axis for brain-tumour treatment. **4l** and **4k** are still in early stages of development. In silico data indicates that both molecules are predicted to be blood–brain barrier penetrant, an important quality for **4k** as a drug treatment for brain cancer. However, both compounds are predicted to be p-glycoprotein substrates, potentially reducing their efficacy as they will be pumped out of the cell with ease. Consequently, further optimisation through carefully designed medicinal chemistry is required before further evaluation in *in-vivo* models. This study has established two novel OTBN-derivatives with promising anti-lung and anti-brain tumour qualities with minimal effect on non-cancerous cells.

## Author contribution

DPV, AA, ADM, HMP and SB contributed to the study concept and design. DPV, MPP, CDP, DBU, SSB and HMP synthesized all compounds and carried characterization and analysis. AA, ADM, JN, and SB carried out the biological evaluations. AG-B, AK and JMP carried out characterisation of compounds in established cancer cell lines. MPP carried out Molecular docking study. DPV, AA, ADM, MPP, JMP, SB and HMP wrote the manuscript. DPV, AA and ADM contributed equally for this work. JMP, HMP, and SB supervised the study and acquired funding. All authors read and approved the final manuscript.

## CRediT authorship contribution statement

**Disha P. Vala:** Conceptualization, Data curation, Formal analysis, Investigation, Methodology, Software, Writing – original draft, Writing – review & editing, Validation. **Amy Dunne Miller:** Conceptualization, Formal analysis, Investigation, Writing – original draft, Writing – review & editing. **Aditi Atmasidha:** Conceptualization, Formal analysis, Methodology, Writing – original draft. **Mehul P. Parmar:** Investigation, Writing – original draft. **Chirag D. Patel:** Data curation. **Dipti B. Upadhyay:** Formal analysis, Investigation. **Savan S. Bhalodiya:** Formal analysis. **Aday González-Bakker:** Data curation, Formal analysis, Investigation, Writing – original draft. **Adam N. Khan:** Formal analysis, Investigation. **Joaquina Nogales:** Conceptualization, Methodology. **José M. Padrón:** Conceptualization, Methodology, Project administration, Supervision, Writing – original draft, Writing – review & editing. **Sourav Banerjee:** Conceptualization, Investigation, Project administration, Supervision, Writing – original draft, Writing – review & editing. **Hitendra M. Patel:** Conceptualization, Investigation, Methodology, Project administration, Supervision, Validation, Writing – original draft, Writing – review & editing.

## Declaration of competing interest

The authors declare that they have no known competing financial interests or personal relationships that could have appeared to influence the work reported in this paper.

## Data availability

Data will be made available on request.

## Appendix A. Supplementary data

Supplementary data to this article can be found online at https://doi.org/10.1016/j.bioorg.2024.107485.

## References

[1] P. Cohen, D. Cross, P.A. Jänne, Kinase drug discovery 20 years after imatinib: progress and future directions, Nat. Rev. Drug Discov. 20 (7) (2021) 551–569, https://doi.org/10.1038/s41573-021-00195-4.

[2] T.P. Heffron, Challenges of developing small-molecule kinase inhibitors for brain tumors and the need for emphasis on free drug levels, Neuro Oncol. 20 (3) (2018) 307–312, https://doi.org/10.1093/neuonc/nox179.

[3] G. Chagoya, S.G. Kwatra, C.W. Nanni, C.M. Roberts, S.M. Phillips, S. Nullmeyergh, S.P. Gilmore, I. Spasojevic, D.L. Corcoran, C.C.J.O. Young, Efficacy of osimertinib against EGFRvIII+ glioblastoma, Oncotarget 11 (22) (2020) 2074, https://doi.org/10.18632/oncotarget.27599.

[4] R. Stupp, W.P. Mason, M.J. van den Bent, M. Weller, B. Fisher, M.J.B. Taphoorn, K. Belanger, A.A. Brandes, C. Marosi, U. Bogdahn, J. Curschmann, R.C. Janzer, S. K. Ludwin, T. Gorlia, A. Allgeier, D. Lacombe, J.G. Cairncross, E. Eisenhauer, R. O. Mirimanoff, Radiotherapy plus concomitant and adjuvant temozolomide for glioblastoma, N. Engl. J. Med. 352 (10) (2005) 987–996, https://doi.org/10.1056/NEJMoa043330.

[5] L.G. Nicely, M. Baxter, S. Banerjee, H. Lord, Sacral ependymoma presents 20 years after initial posterior fossa lesion, BMJ Case Rep. 16 (10) (2023), https://doi.org/10.1136/bcr-2023-256611.

[6] A. Keenlyside, T. Marples, Z. Gao, H. Hu, L.G. Nicely, J. Nogales, H. Li, L. Landgraf, A. Solth, A. Melzer, K. Hossain-Ibrahim, Z. Huang, S. Banerjee, J. Joseph,

Development and optimisation of in vitro sonodynamic therapy for glioblastoma, Sci. Rep. 13 (1) (2023) 20215, https://doi.org/10.1038/s41598-023-47562-2.

[7] V.V. Rostovtsev, L.G. Green, V.V. Fokin, K.B. Sharpless, A stepwise huisgen cycloaddition process: copper(I)-catalyzed regioselective "Ligation" of azides and terminal alkynes, Angew. Chem. Int. Ed. 41 (14) (2002) 2596–2599, https://doi.org/10.1002/1521-3773(20020715)41:14<2596::AID-ANIE2596>3.0.CO;2-4.

[8] C.W. Tornøe, C. Christensen, M. Meldal, Peptidotriazoles on solid phase: [1,2,3]-triazoles by regiospecific copper(I)-catalyzed 1,3-dipolar cycloadditions of terminal alkynes to azides, J. Org. Chem. 67 (9) (2002) 3057–3064, https://doi.org/10.1021/jo011148j.

[9] D.P. Vala, R.M. Vala, H.M. Patel, Versatile synthetic platform for 1,2,3-triazole chemistry, ACS Omega 7 (42) (2022) 36945–36987, https://doi.org/10.1021/acsomega.2c04883.

[10] N. Ma, Y. Wang, B.-X. Zhao, W.-C. Ye, S. Jiang, The application of click chemistry in the synthesis of agents with anticancer activity, Drug Des., Dev. Ther. 9 (2015) 1585–1599, https://doi.org/10.2147/DDDT.S56038.

[11] R.M. Vala, M.G. Sharma, D.M. Patel, A. Puerta, J.M. Padrón, V. Ramkumar, R.L. Gardas, H.M. Patel, Synthesis and in vitro study of antiproliferative benzyloxy dihydropyrimidinones, Arch. Pharm. 354 (6) (2021) 2000466, https://doi.org/10.1002/ardp.202000466.

[12] N. Patel, S. Pathan, H.I. Soni, 3,4-Dihydropyrimidin-2(1H)-one analogues: microwave irradiated synthesis with antimicrobial and antituberculosis study, Curr. Microwave Chem. 6 (1) (2019) 61–70, https://doi.org/10.2174/2213335606666190724093305.

[13] M.P. Parmar, R.M. Vala, H.M. Patel, Importance of hybrid catalysts toward the synthesis of 5H-pyrano[2,3-d]pyrimidine-2-ones/2,4-diones (Thiones), ACS Omega 8 (2) (2023) 1759–1816, https://doi.org/10.1021/acsomega.2c05349.

[14] D.B. Upadhyay, J.A. Mokariya, P.J. Patel, S.G. Patel, A. Das, A. Nandi, J. Nogales, N. More, A. Kumar, D.P. Rajani, M. Narayan, J. Kumar, S. Banerjee, S.K. Sahoo, H.M. Patel, Indole clubbed 2,4-thiazolidinedione linked 1,2,3-triazole as a potent antimalarial and antibacterial agent against drug-resistant strain and molecular modeling studies, Arch. Pharm. (2024) e2300673.

[15] D.M. Patel, M.G. Sharma, R.M. Vala, I. Lagunes, A. Puerta, J.M. Padrón, D.P. Rajani, H.M. Patel, Hydroxyl alkyl ammonium ionic liquid assisted green and one-pot regioselective access to functionalized pyrazolodihydropyridine core and their pharmacological evaluation, Bioorg. Chem. 86 (2019) 137–150, https://doi.org/10.1016/j.bioorg.2019.01.029.

[16] Z.J. Jain, P.S. Gide, R.S. Kankate, Biphenyls and their derivatives as synthetically and pharmacologically important aromatic structural moieties, Arab. J. Chem. 10 (2017) S2051–S2066, https://doi.org/10.1016/j.arabjc.2013.07.035.

[17] K. Banert, Reactions of Unsaturated Azides, 6. Synthesis of 1,2,3-Triazoles from Propargyl Azides by Rearrangement of the Azido Group. – Indication of Short-Lived Allenyl Azides and Triazafulvenes, Ber. 122 (5) (1989) 911–918, https://doi.org/10.1002/cber.19891220520.

[18] K. Bozorov, J. Zhao, H.A. Aisa, 1,2,3-Triazole-containing hybrids as leads in medicinal chemistry: A recent overview, Bioorg. Med. Chem. 27 (16) (2019) 3511–3531, https://doi.org/10.1016/j.bmc.2019.07.005.

[19] N.J. Agard, J.A. Prescher, C.R. Bertozzi, A strain-promoted [3 + 2] azide-alkyne cycloaddition for covalent modification of biomolecules in living systems, J. Am. Chem. Soc. 126 (46) (2004) 15046–15047, https://doi.org/10.1021/ja044996f.

[20] S. Hakimian, A. Cheng-Hakimian, G.D. Anderson, J.W. Miller, Rufinamide: a new anti-epileptic medication, Expert Opin. Pharmacother. 8 (12) (2007) 1931–1940, https://doi.org/10.1517/14656566.8.12.1931.

[21] E. Bonandi, M.S. Christodoulou, G. Fumagalli, D. Perdicchia, G. Rastelli, D. Passarella, The 1, 2, 3-triazole ring as a bioisostere in medicinal chemistry, Drug Discov. Today 22 (10) (2017) 1572–1581, https://doi.org/10.1016/j.drudis.2017.05.014.

[22] M. Sharkey, N. Sharova, I. Mohammed, S.E. Huff, I.R. Kummetha, G. Singh, T.M. Rana, M. Stevenson, HIV-1 Escape from Small-Molecule Antagonism of Vif, MBio 10 (1) (2019) e00144–e00219, https://doi.org/10.1128/mbio.00144-19.

[23] C. Scholl, S. Fröhling, I.F. Dunn, A.C. Schinzel, D.A. Barbie, S.Y. Kim, S.J. Silver, P. Tamayo, R.C. Wadlow, S.J.C. Ramaswamy, Synthetic lethal interaction between oncogenic KRAS dependency and STK33 suppression in human cancer cells, Cell 137 (5) (2009) 821–834, https://doi.org/10.1016/j.cell.2009.03.017.

[24] T. Luo, K. Masson, J.D. Jaffe, W. Silkworth, N.T. Ross, C.A. Scherer, C. Scholl, S. Fröhling, S.A. Carr, A.M. Stern, S.L. Schreiber, T.R. Golub, STK33 kinase inhibitor BRD-8899 has no effect on KRAS-dependent cancer cell viability, Proc. Natl. Acad. Sci. 109 (8) (2012) 2860–2865, https://doi.org/10.1073/pnas.1120589109.

[25] M.B. Davies, Reactions of L-ascorbic acid with transition metal complexes, Polyhedron 11 (3) (1992) 285–321, https://doi.org/10.1016/S0277-5387(00)83175-7.

[26] K. Bhagat, J. Bhagat, M.K. Gupta, J.V. Singh, H.K. Gulati, A. Singh, K. Kaur, G. Kaur, S. Sharma, A. Rana, H. Singh, S. Sharma, P.M. Singh Bedi, Design, Synthesis, Antimicrobial Evaluation, and Molecular Modeling Studies of Novel Indolinedione-Coumarin Molecular Hybrids, ACS Omega 4 (5) (2019) 8720–8730, https://doi.org/10.1021/acsomega.8b02481.

[27] Puerta A, Galán AR, Abdilla R, Demanuele K, Fernandes MX, Bosica G, Padrón JM, Naphthol-derived Betti bases as potential SLC6A14 blockers, J. Mol. Clin. Med. 2 (2) (2019) 35–40, https://doi.org/10.31083/j.jmcm.2019.02.7181.

[28] J. Klughammer, B. Kiesel, T. Roetzer, N. Fortelny, A. Nemc, K.-H. Nenning, J. Furtner, N.C. Sheffield, P. Datlinger, N. Peter, M. Nowosielski, M. Augustin, M. Mischkulnig, T. Ströbel, D. Alpar, B. Ergüner, M. Senekowitsch, P. Moser, C.F. Freyschlag, J. Kerschbaumer, C. Thomé, A.E. Grams, G. Stockhammer, M. Kitzwogerer, S. Oberndorfer, F. Marhold, S. Weis, J. Trenkler, J. Buchroithner, J. Pichler, J. Haybaeck, S. Krassnig, K. Mahdy Ali, G. von Campe, F. Payer,

C. Sherif, J. Preiser, T. Hauser, P.A. Winkler, W. Kleindienst, F. Würtz, T. Brandner-Kokalj, M. Stultschnig, S. Schweiger, K. Dieckmann, M. Preusser, G. Langs, B. Baumann, E. Knosp, G. Widhalm, C. Marosi, J.A. Hainfellner, A. Woehrer, C. Bock, The DNA methylation landscape of glioblastoma disease progression shows extensive heterogeneity in time and space, Nat. Med. 24 (10) (2018) 1611–1624, https://doi.org/10.1038/s41591-018-0156-x.

[29] A. Daina, V. Zoete, A BOILED-Egg To Predict Gastrointestinal Absorption and Brain Penetration of Small Molecules, ChemMedChem 11 (11) (2016) 1117–1121, https://doi.org/10.1002/cmdc.201600182.

[30] J.M. Roldán-Peña, A. Puerta, J. Dinić, S. Jovanović Stojanov, A. González-Bakker, F.J. Hicke, A. Mishra, A. Piyasaengthong, I. Maya, J.W. Walton, M. Pešić, J.M. Padrón, J.G. Fernández-Bolaños, Ó. López, Biotinylated selenocyanates: Potent and selective cytostatic agents, Bioorg. Chem. 133 (2023) 106410, https://doi.org/10.1016/j.bioorg.2023.106410.

[31] M.C. Padilla-Pérez, E.M. Sánchez-Fernández, A. González-Bakker, A. Puerta, J.M. Padrón, F. Martín-Loro, A.I. Arroba, J.M. García Fernández, C.O. Mellet, Fluoro-labelled sp2-iminoglycolipids with immunomodulatory properties, Eur. J. Med. Chem. 255 (2023) 115390, https://doi.org/10.1016/j.ejmech.2023.115390.

[32] R.E. Barrientos, E. Ibáñez, A. Puerta, J.M. Padrón, A. Paredes, F. Cifuentes, J. Romero-Parra, J. Palacios, J. Bórquez, M.j., Simirgiotis phenolic fingerprinting and bioactivity profiling of extracts and isolated compounds from Gypothamnium pinifolium Phil, Antioxidants 11 (2022), https://doi.org/10.3390/antiox11122313.

[33] A. Alguacil, F. Scalambra, P. Lorenzo-Luis, A. Puerta, A. González-Bakker, Z. Mendoza, J.M. Padrón, A. Romerosa, Tetranuclear Ru2Cu2 and Ru2Ni2 complexes with nanomolar anticancer activity, Dalton Trans. 52 (28) (2023) 9541–9545, https://doi.org/10.1039/D3DT01284K.

[34] R. Lacret, A. Puerta, S. Granica, A. González-Bakker, D. Hevia, Y. Teng, C.C. Sánchez-Mateo, P.L. Pérez de Paz, J.m., Padrón bioactive potential: a pharmacognostic definition through the screening of four hypericum species from the Canary Islands, Molecules 27 (2022) 6101, https://doi.org/10.3390/molecules27186101.

[35] S.-G. Zhao, X.-F. Chen, L.-G. Wang, Y. Gang, D.-Y. Han, L. Teng, M.-C. Yang, D.-Y. Wang, C. Shi, Y.-H. Liu, B.-J. Zheng, C.-B. Shi, X. Gao, N.G. Rainov, Increased expression of ABCB6 enhances protoporphyrin IX accumulation and photodynamic effect in human glioma, Ann. Surg. Oncol. 20 (13) (2013) 4379–4388, https://doi.org/10.1245/s10434-011-2201-6.

[36] S. Banerjee, C. Ji, J.E. Mayfield, A. Goel, J. Xiao, J.E. Dixon, X. Guo, Ancient drug curcumin impedes 26S proteasome activity by direct inhibition of dual-specificity tyrosine-regulated kinase 2, Proc. Natl. Acad. Sci. 115 (32) (2018) 8155–8160, https://doi.org/10.1073/pnas.1806797115.

[37] S. Banerjee, S.J. Buhrlage, H.-T. Huang, X. Deng, W. Zhou, J. Wang, R. Traynor, A.R. Prescott, D.R. Alessi, N.S. Gray, Characterization of WZ4003 and HTH-01-015 as selective inhibitors of the LKB1-tumour-suppressor-activated NUAK kinases, Biochem. J 457 (1) (2013) 215–225, https://doi.org/10.1042/BJ20131152.

[38] S. Banerjee, T. Wei, J. Wang, J.J. Lee, H.L. Gutierrez, O. Chapman, S.E. Wiley, J.E. Mayfield, V. Tandon, E.F. Juarez, L. Chavez, R. Liang, R.L. Sah, C. Costello, J.P. Mesirov, L. de la Vega, K.L. Cooper, J.E. Dixon, J. Xiao, X. Lei, Inhibition of dual-specificity tyrosine phosphorylation-regulated kinase 2 perturbs 26S proteasome-addicted neoplastic progression, Proc. Natl. Acad. Sci. 116 (49) (2019) 24881–24891, https://doi.org/10.1073/pnas.1912033116.

[39] V. Tandon, R.M. Vala, A. Chen, R.L. Sah, H.M. Patel, M.C. Pirrung, S. Banerjee, Syrbactin-class dual constitutive- and immuno-proteasome inhibitor TIR-199 impedes myeloma-mediated bone degeneration in vivo, p. BSR20212721, Biosci. Rep. 42 (2) (2022), https://doi.org/10.1042/BSR20212721.

[40] J. Jumper, R. Evans, A. Pritzel, T. Green, M. Figurnov, O. Ronneberger, K. Tunyasuvunakool, R. Bates, A. Žídek, A. Potapenko, A. Bridgland, C. Meyer, S.A.A. Kohl, A.J. Ballard, A. Cowie, B. Romera-Paredes, S. Nikolov, R. Jain, J. Adler, T. Back, S. Petersen, D. Reiman, E. Clancy, M. Zielinski, M. Steinegger, M. Pacholska, T. Berghammer, S. Bodenstein, D. Silver, O. Vinyals, A.W. Senior, K. Kavukcuoglu, P. Kohli, D. Hassabis, Highly accurate protein structure prediction with AlphaFold, Nature 596 (7873) (2021) 583–589, https://doi.org/10.1038/s41586-021-03819-2.

[41] V. Tandon, R. Moreno, K. Allmeroth, J. Quinn, S.E. Wiley, L.G. Nicely, M.S. Denzel, J. Edwards, L. de la Vega, S. Banerjee, Dual inhibition of HSF1 and DYRK2 impedes cancer progression, p. BSR20222102, Biosci. Rep. 43 (1) (2023), https://doi.org/10.1042/BSR20222102.

[42] R.M. Vala, V. Tandon, L.G. Nicely, L. Guo, Y. Gu, S. Banerjee, H.M. Patel, Synthesis of N-(4-chlorophenyl) substituted pyrano[2,3-c]pyrazoles enabling PKBβ/AKT2 inhibitory and in vitro anti-glioma activity, Ann. Med. 54 (1) (2022) 2548–2560, https://doi.org/10.1080/07853890.2022.2123559.

[43] L.G. Nicely, R.M. Vala, D.B. Upadhyay, J. Nogales, C. Chi, S. Banerjee, H.M. Patel, One-pot two-step catalytic synthesis of 6-amino-2-pyridone-3, 5-dicarbonitriles enabling anti-cancer bioactivity, RSC Adv. 12 (37) (2022) 23889–23897, https://doi.org/10.1039/D2RA03579K.

[44] F. Kong, X. Kong, Y. Du, Y. Chen, X. Deng, J. Zhu, J. Du, L. Li, Z. Jia, D. Xie, Z. Li, K. Xie, STK33 promotes growth and progression of pancreatic cancer as a critical downstream mediator of HIF1α, Cancer Res. 77 (24) (2017) 6851–6862, https://doi.org/10.1158/0008-5472.CAN-17-0067.

[45] S. Zhang, H. Wu, K. Wang, M. Liu, STK33/ERK2 signal pathway contribute the tumorigenesis of colorectal cancer HCT15 cells, p. BSR20182351, Biosci. Rep. 39 (3) (2019), https://doi.org/10.1042/BSR20182351.

[46] Y. Lu, J. Tang, W. Zhang, C. Shen, L. Xu, D. Yang, Correlation between STK33 and the pathology and prognosis of lung cancer, Oncol. Lett. 14 (4) (2017) 4800–4804, https://doi.org/10.3892/ol.2017.6766.

[47] D.M. Quddusi, N. Bajcinca, Identification of genomic biomarkers and their pathway crosstalks for deciphering mechanistic links in glioblastoma, IEE Syst. Biol. 17 (4) (2023) 143–161, https://doi.org/10.1049/syb2.12066.